JOURNAL OF APPLIED ELECTROCHEMISTRY 19 (1989) 571–579

Mass transfer and structure of asbestos and non-asbestos diaphragms for chlorine and caustic production*

IR. J. H. G. VAN DER STEGEN

AKZO Salt and Basic Chemicals Nederland B.V., Boortorenweg 20, PO Box 25, 7550 GC Hengelo, The Netherlands

Received August 1988; revised 1 December 1988

Models and equations describing aspects of diaphragm performance are discussed in view of recent experiences with non-asbestos diaphragms. Excellent control of wettability and, therefore, of the amount of gases inside the diaphragm, together with chemical resistance to the environment during electrolysis, was found to be an essential prerequisite to performances of non-asbestos diaphragms that are comparable to those of asbestos diaphragms. Equations, derived and supported by experimental evidence from previous work, are shown to describe and predict hydrodynamic permeability and ohmic voltage drop of diaphragms, even in cases where the amount of gases inside the diaphragm slowly increases during electrolysis. Current efficiency is observed to be only dependent to a slight extent on the effective electrolyte void fraction inside the diaphragm. Major effects that determine current efficiency at $2\,kA\,m^{-2}$ and $120\,g\,l^{-1}$ caustic are shown to be diaphragm thickness, pore diameter distribution and the number of interconnections between pores inside the diaphragm. A discussion on design of the structure of non-asbestos diaphragms is presented.

Nomenclature

B	permeability coefficient (m^2)
$c_{i,x}$	concentration of ionic species i at position x ($mol\,m^{-3}$)
c_k	concentration of hydroxyl ions in catholyte ($mol\,m^{-3}$)
CE	current efficiency
d	thickness of diaphragm (m)
β	thickness of layer (m)
D_i	ionic diffusion coefficient of species i ($m^2\,s^{-1}$)
D_e	dispersion coefficient ($m^2\,s^{-1}$)
ε	electrolyte void fraction
E	potential inside diaphragm (V)
F	Faraday constant, 96 487 ($C\,mol^{-1}$ of electrons)
$F_{j,i}$	flux of ionic species i in the stagnant electrolyte inside small pores of layer j
H	hydrostatic head ($N\,m^{-2}$)
i	flux of current $= j/F$ ($mol\,m^{-2}\,s^{-1}$)
j	current density ($A\,m^{-2}$)
$k_{i,1}$	constant representing diffusion in diaphragm ($m^2\,s^{-1}$)
k_2	constant representing migration in diaphragm (m^{-1})
v_p	hydraulic pore radius according to [15] (m)
N	number of layers
$N_{j,i}$	flux of ionic species i in layer j ($mol\,m^{-2}\,s^{-1}$)
P	hydrodynamic permeability ($m^3\,N^{-1}\,s^{-1}$)
R	gas constant, 8.3143 ($J\,mol^{-1}\,K^{-1}$)
ϱ	density of liquid ($kg\,m^{-3}$)
R_0	electric resistivity of electrolyte (ohm m)
R_d	electric resistivity of porous structure filled with electrolyte (ohm m)
R_m	resistance of the diaphragm (ohm m^2)
R_a	resistance of anolyte layer (ohm m^2)
R_e	resistance of electrodes (ohm m^2)
s	specific surface of porous structure (m^{-1})
s_0	standard specific surface of solids in porous structure (m^{-1})
τ	tortuosity defined according to $R_d/R_0 = \tau/\varepsilon$
T	absolute temperature (K)
u	superficial liquid velocity ($m\,s^{-1}$)
U	cell voltage (V)
η	dynamic viscosity ($N\,s\,m^{-2}$)
ν	kinematic viscosity ($m^2\,s^{-1}$)
x	diaphragm dimensional coordinate (m)
y	radial coordinate inside pores (m)

1. Introduction

Chemical resistance to attack by chlorine or caustic soda in the environment for chloralkali production and problems caused by the poor wettability of PTFE, which is a polymer with excellent chemical resistance, have been major problems for 20 years in the development of non-asbestos diaphragms. This hurdle on the

* Paper presented at the meeting on Materials Problems and Material Sciences in Electrochemical Engineering Practice organised by the Working Party on Electrochemical Engineering of the European Federation of Chemical Engineers held at Maastricht, The Netherlands, September 17th and 18th 1987.

0021-891X/89 $03.00 + .12

road to long-lasting steady performance, at performances comparable to those of the asbestos diaphragm, is now reported to be overcome [1, 2]. Both Leysen and Vermeiren [1] and Curlin [2] report such results for 100 days and more on diaphragms consisting of zirconia and PTFE.

The purpose of this paper is to offer a description of the major performance criteria, current efficiency, cell voltage and hydrodynamic permeability, of this non-asbestos diaphragm technology for chlorine caustic production.

Their predecessor, the asbestos diaphragm, which is expected to eventually be replaced, has been in operation in numerous plants since 1924 and until today with reasonably good performance. However, asbestos is an environmental and health hazard and, moreover, it is not perfect in its chemical stability.

2. Economics of non-asbestos diaphragm development

Cells with asbestos or non-asbestos diaphragms have to compete with mercury or membrane cells in chlorine caustic production. The economy of a technically successful development may thus be questionable.

New capacities installed in Western Europe, the USA and Japan since 1984 are without exception based on membrane cell technology. Membrane cell technology is economically and technically superior to the two older technologies. However, differences in totals of production costs between the three processes are less than 10% of the total of chlorine production costs [3, 4] and thus the process of conversion will still go on slowly for a long time. From Fig. 1 it is estimated that this process could take 30 years until all diaphragm cells are replaced by membrane cells.

3. Description of chlorine caustic diaphragm cell technology

Cells with asbestos diaphragms have been in operation since 1924 and several excellent surveys on their performance and operation exist [5–7].

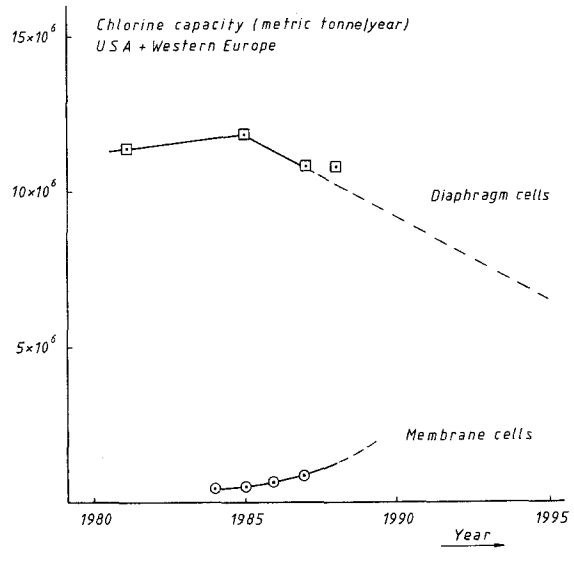

Fig. 1. Chlorine production capacities in diaphragm and membrane cells of Western Europe and the United States versus time.

Asbestos diaphragms are deposited from a slurry of asbestos fibres in diaphragm liquor (12% caustic and 14% sodium chloride dissolved in water) on an iron cathode screen. Under the electron microscope they are found to consist of a chaos of fibres with diameters in the order of 1 μm.

Curlin [2] reported on diaphragms deposited in a highly similar manner from a slurry of pretreated PTFE fibres. Before deposition on the cathode screen these fibres are pretreated with zirconia powder, in order to obtain the wettability needed for proper cell performance. SEM photographs show PTFE fibres carrying a surface cover of zirconia particles [2].

Leysen and Vermeiren [1] reported on a porous PTFE sheet diaphragm which contains a considerable amount of zirconia. These porous sheets are manufactured by mixing PTFE particles, zirconia powder and a powder of a soluble component. Mixing of components is followed by rolling, pressing and curing of the mixture. After leaching the soluble component, a porous PTFE sheet, which is wettable due to the zirconia, is obtained.

Applicability of non-asbestos diaphragms in existing cells is a further point of economic interest. In case of non-fulfilment of this criterion, new investments in cathode and anode structure become necessary, and investment in new membrane cells would be more likely.

Fulfilling this applicability criterion thus required further research and development. As both sheet-type non-asbestos diaphragms and fibrous non-asbestos diaphragms are proposed, typical solutions to both types are reported. One solution for the mounting of a sheet diaphragm into an existing cell is described by Kadija [8], Byrd [9] and Krause [10]. Additional equipment and auxiliaries are necessary.

At first glance at the second type, it appears that fibre diaphragms may be deposited in a similar manner to asbestos diaphragms onto the cathode screen. However, the density of the PTFE/zirconia mixture is reported to be twice the density of asbestos and, moreover, fibre length and diameter of the Polyramix fibre is reported [2] to be much larger than the corresponding dimensions of asbestos. These PTFE/zirconia fibres will thus sediment in diaphragm liquor at a much higher rate than asbestos fibres. And, thus, in the case of Polyramix, additional equipment and auxiliaries are needed to maintain stability of the slurry during deposition of the diaphragm.

In diaphragm cells brine (305 g l^{-1}, 60–80° C, pH 4–7) is fed into the anode compartment of the cell. At the anode chlorine is evolved according to

$$2Cl^- \longrightarrow Cl_2 + 2e^-$$

The diaphragm separates the anode compartment from the cathode compartment. At the cathode hydrogen is produced according to

$$2H_2O + 2e^- \longrightarrow H_2 + 2OH^-$$

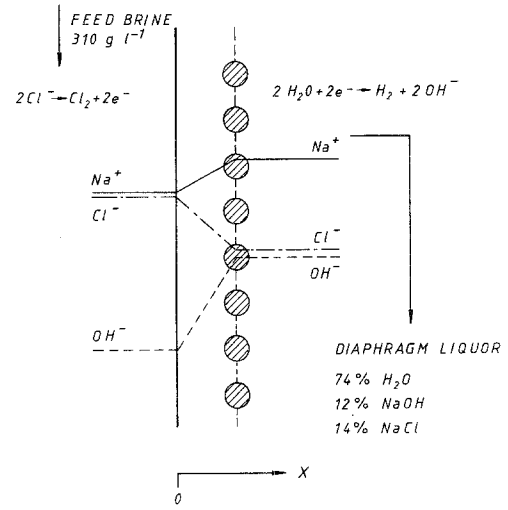

Fig. 2. Schematic view of the diaphragm and the concentration profiles across the diaphragm in a chloralkali electrolysis cell.

Hydroxyl ions tend to move down the concentration gradient from catholyte to anolyte and, moreover, migration due to electric current forces them in the same direction. This movement of the hydroxyl ions is countered by the flow of electrolyte directed from anolyte towards catholyte.

Concentration profiles of ions, together with basic reactions, are shown in Fig. 2. It should be noted that the x axis of the diaphragm is defined as the direction of the electrolyte flow from anolyte to catholyte. At the anodic face of the diaphragm x is zero.

From all further details, as described by Hine [5], Caldwell [6] and Kirchner [7], it should be stressed that electrolyte flow counters the effect of migration and diffusion of hydroxyl ions. Thus brine flow rate is, together with other parameters, current efficiency determining.

Table 1 presents typical operating and performance data of asbestos diaphragms. In order to be economically successful non-asbestos diaphragms should beat these performance data.

4. Basic equations describing diaphragm performance

4.1. *Cell voltage and hydrodynamic permeability*

A diaphragm is a porous system filled with electrolyte and, thus, formulae describing conductivity of porous systems are applicable to diaphragms. Meredith and Tobias [14] presented a review of such equations.

Table 1. Typical operating and performance data of asbestos diaphragms

Current density	$2\,kA\,m^{-2}$
Conversion	0.5–0.55 mol NaOH/mol NaCl in feed
Current efficiency	95–97%
Cell voltage	2.9 V (anode–cathode)
Permeability range	$1–2 \times 10^{-9} m^3 N^{-1} s^{-1}$
Hydrogen in chlorine	< 0.2%
Life time	10–14 months
Caustic strength	$120–140\,g\,l^{-1}$

From this review the Bruggeman [13] equation is chosen to describe diaphragm resistance

$$R_d/R_0 = \varepsilon^{-1.5} \quad (1)$$

MacMullin and Muccini [15] tested this equation at void fractions from 20–40% and reported an error of $\pm 10\%$.

Diaphragm resistance is described by

$$R_m = R_d d = R_0 d\varepsilon^{-1.5} \quad (2)$$

According to MacMullin and Muccini [15] the permeability coefficient, B, and the electric resistance of porous systems are related by the equation

$$(\varepsilon/s)^2 = v_p^2 = kBR_d/R_0 = kB\varepsilon^{-1.5} \quad (3)$$

According to this equation diaphragm resistance, and thus cell voltage, will increase, all other parameters being constant, for a decrease of the permeability coefficient. Equation 3 leaves only one parameter to influence the product of diaphragm resistance and permeability coefficient, i.e. the hydraulic pore radius.

The constant k is equal to 3.666 ± 0.098. By definition the permeability coefficient, B, is related to hydrodynamic permeability according to

$$B = P\{d\eta\}$$

Substituting the permeability coefficient by the hydrodynamic permeability gives

$$P = B\{d\eta\}^{-1} = v_p^2 R_0/R_d k^{-1}\{d\eta\}^{-1} \quad (4)$$

4.2. *Current efficiency*

As any loss of hydroxyl ions by movement from catholyte to anolyte is loss of product, current efficiency based on sodium hydroxide is given by

$$CE = (1 - FN_{3,x} j^{-1}) \times 100 \quad (5)$$

The flux of hydroxyl ions at any position inside the diaphragm is given [5, 16] by

$$N_{3,x} = u_x c_{3,x} - D_3 \frac{\partial c_{3,x}}{\partial x} - D_3 c_{3,x} \frac{F}{RT} \frac{\partial E}{\partial x} \quad (6)$$

$N_{3,x}$ represents the flux of hydroxyl ions at position x whereas $c_{3,x}$ represents concentration of hydroxyl ions at position x. Subscript 1 stands for sodium ions, 2 for chloride and 3 for hydroxyl ions.

Mukaibo [12] derived a solution to Equation 6 and Hine [5] presented experimental data to support this solution. According to Mukaibo, current efficiency is given by

$$CE = \frac{100u}{\{u + (n_0 i - u)/a_1\}} \quad (7)$$

$$a_1 = 1 - \exp \frac{[-(n_0 i - u)d]}{k_0}$$

$$k_0 = 1.62 \times 10^{-9} m^2 s^{-1}$$

$$n_0 = 200–250$$

This equation was tested against results on asbestos

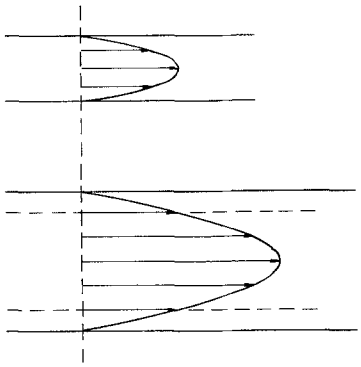

Fig. 3. Velocity profile inside pores at laminar flow.

diaphragms ranging in thickness from 2.1 to 8.5 mm and Hine [5] reported agreement.

As liquid velocity (u) and current density (j) are chosen on economic considerations, this Equation 7 leaves only one parameter to influence current efficiency, i.e. diaphragm thickness (d).

Recently, in their simple model of diaphragms, another solution of Equation 6 was derived by White *et al.* [17]. Current efficiency was shown to depend on the product of diaphragm thickness and the tortuosity of the pores inside the diaphragm. Only in the case that a value of $R_d/R_0 = 1.52$ was entered into their solution could these authors obtain agreement between experimental results on the asbestos diaphragms of Hine [5] and their predictions.

Lazarz [18] studied non-asbestos diaphragms of different thicknesses. She reported, for example on 1.4 mm diaphragms, results on current efficiency ranging from 75 to 98%. Thus Lazarz judged Equation 7 unable to explain all observations on non-asbestos diaphragms. Pore diameter distribution was introduced to explain these new phenomena.

In order to further stress this point Fig. 3 presents the well-known parabolic liquid velocity distribution inside pores of different diameters. At the wall the velocity is zero: in the centre of the pore velocity is high. Velocity increases with diameter of the pore. Thus, according to Equation 6, at those positions where the velocity is low diffusion and migration govern the movement of hydroxyl ions. At those positions hydroxyl ions move towards the anolyte, whereas at those positions where the velocity is high hydroxyl ions are flushed backwards to the catholyte.

Lazarz [18] was the first to discuss pore diameter distribution. Her considerations are important because they question the use of the superficial liquid velocity as a unique parameter in Equation 6 as done by Mukaibo [5] and by White *et al.* [17]. Attempts to solve Equation 6, keeping in mind the liquid velocity distribution at any position inside the diaphragm, should be made.

5. Observations on asbestos and non-asbestos diaphragms

Hine [5] reported numerous data on the performance of asbestos diaphragms. Based on the observed rapid changes of electric resistance and of the liquid permeability Hine suggested the existence of hydrogen bubbles inside the diaphragm. In his opinion a modified asbestos diaphragm is to be treated as a four-phase system, consisting of asbestos, modifier (PTFE or Halar), electrolyte and hydrogen bubbles.

If suggestions by Hine are accepted, then electric resistance and permeability of asbestos diaphragms are to be described with the aid of an effective electrolyte void fraction. This effective electrolyte void fraction is equal to the volume fraction not occupied by solids minus the gas void fraction and minus the volume of electrolyte in dead end pores. Fortunately, as shown by electron microscope, asbestos diaphragms and most non-asbestos diaphragms do not contain such dead end pores. As the content of hydrogen bubbles increases then electrolyte void fraction decreases and, thus, according to Equation 2 diaphragm electrical resistance then increases and, according to Equation 4, hydrodynamic permeability then decreases.

In well-performing non-asbestos diaphragms, such as those described by Leysen and Vermeiren [1] and Curlin [2], the gas void is relatively low and constant with time. Only in poor diaphragms does the gas void fraction change with time. Although they are, from an industrial viewpoint, unimportant, such poor diaphragms offer a unique possibility of investigating the influence of the effective electrolyte void fraction, all other parameters being constant, on current efficiency.

Figure 4 presents results on such a poor diaphragm, which was a commercially available porous PTFE sheet with an average pore diameter of 5 μm. This sheet was, due to its poor wettability with the electrolyte, impermeable to the electrolyte. Pretreatment with a surfactant is a well-known procedure to overcome this problem. Thus, treatment with Zonyl FSN solution was employed to obtain the desired filling with electrolyte. Electrolysis at 2 kA m^{-2} with a brine flow rate producing 120 g l^{-1} caustic was started.

From Fig. 4, an increase of cell voltage, a decrease of hydrodynamic permeability and a slight decrease of current efficiency with time and increasing cell voltage are observed. As all other parameters are constant, the only remaining explanation of the increasing cell voltage is the increase in diaphragm electric resistance, and thus an increase of the ratio R_d/R_0. Increase of the ratio R_d/R_0 is explained according to Equation 1 by decrease of the effective electrolyte void fraction. This observation and its explanation is important because of the paper on the simple model of the diaphragm in which Van Zee and White [16] have shown that current efficiency increases with increase of the product of the ratio R_d/R_0 and diaphragm thickness. Thus current efficiency, in the experiment of Fig. 4, is expected, according to their model, to increase during this experiment. The observations, as shown in Fig. 4, and the simple model [16, 17] are thus in contradiction.

Cell voltage, as shown, was found to increase slowly with time whereas hydrodynamic permeability slowly

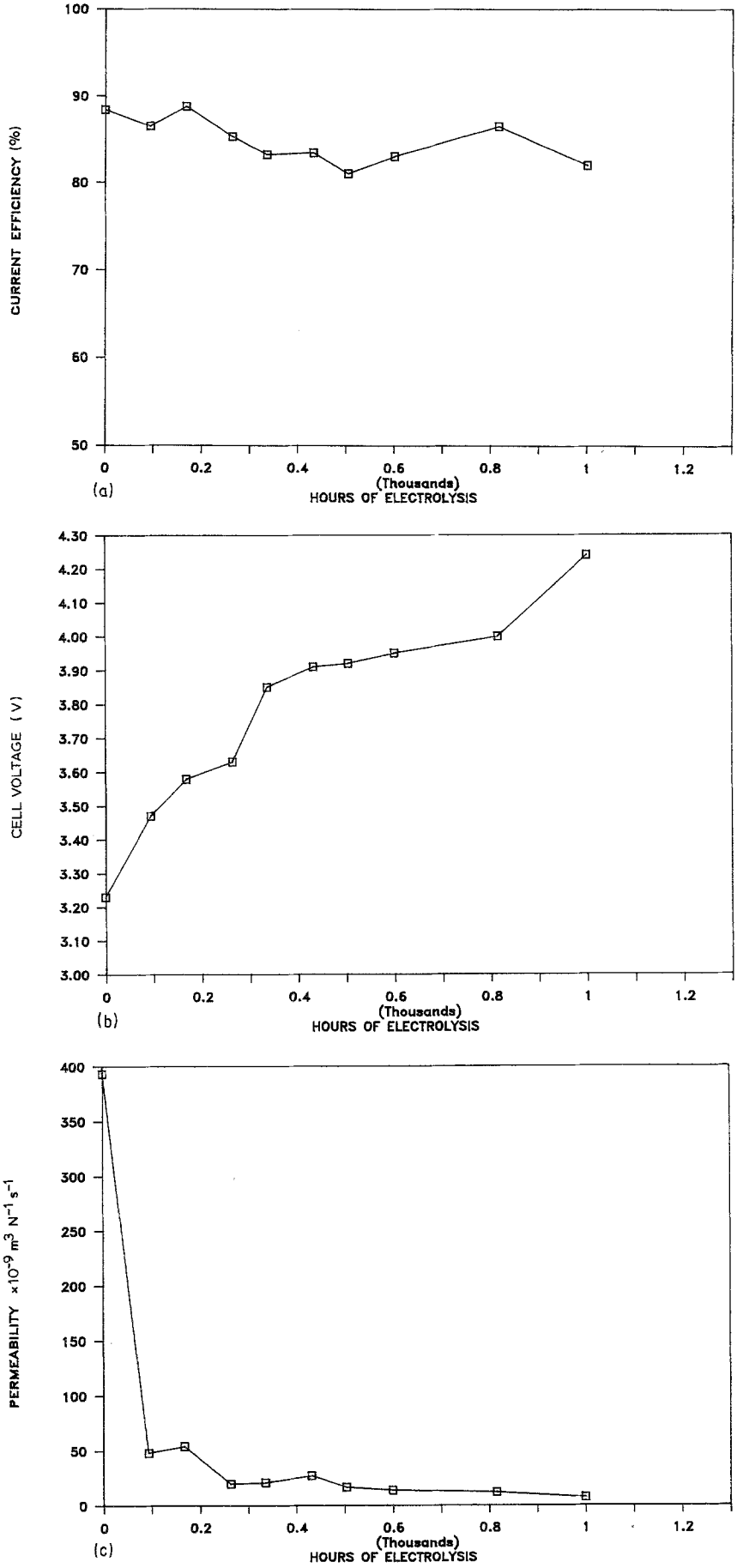

Fig. 4. Cell voltage, hydrodynamic permeability and current efficiency of a porous PTFE diaphragm after pretreatment with Zonyl FSN versus time of electrolysis.

decreased. These observations are explained in a physicochemical manner by a slow dissolution of the surfactant. As the amount of surfactant decreases, the non-wetting properties of PTFE become more apparent. Thus the volume fraction of hydrogen gas inside the diaphragm starts to increase. Similar observations on porous PTFE are described by Lazarz [19] and Bachot [11]. In fact, by weighing asbestos or non-

asbestos diaphragms in a specially designed electrolysis cell, the author was able to gain additional evidence on accumulation of hydrogen gas within the diaphragm.

Thus asbestos and non-asbestos diaphragms may be described with the aid of an effective electrolyte void fraction. This effective electrolyte void fraction is equal to the volume fraction not occupied by solids minus the gas void fraction.

6. Changing the effective electrolyte void fraction. A more detailed mathematical description of diaphragm performance

6.1. *Cell voltage and hydrodynamic permeability*

One purpose of this paper is to compare observations on diaphragms, as shown in Fig. 4, with expectations based on the basic equations which describe diaphragm performance. Firstly, the (time-dependent) value of the diaphragm resistance is obtained from the observed cell voltage according to

$$U = U_0 + (R_a + R_m + R_e)j \tag{8}$$

U_0 represents the sum of the reversible electrode potentials plus overvoltages. R_a, R_m and R_e represent the ohmic resistances of anolyte, diaphragm and electrodes and j represents current density. U, U_0, R_a, R_e and j are constants during the experiment. These parameters are either known or are measured or derived from the set of experimental data. Then, according to Equation 2 the (time-dependent) effective electrolyte void fraction can be calculated. In order to calculate the (time-dependent) hydrodynamic permeability according to Equation 4, another parameter, the (time-dependent) hydraulic pore radius, has to be known.

The hydraulic radius v_p is defined by MacMullin and Muccini [15] as

$$v_p = \varepsilon/s \tag{9}$$

As hydrogen gas slowly replaces electrolyte with time, not only the electrolyte void fraction (ε), but also the specific surface (s) is time dependent. Thus it is important to introduce a specific surface area of the electrolyte that depends on effective electrolyte void fraction.

$$s = s_0\varepsilon(1 - \varepsilon) \tag{10}$$

s_0 is the standard specific surface of the porous structure, which is a constant of the structure under investigation. Its value can be obtained by introducing the result of BET measurements as s and the volume fraction of non-solids of the dry sample as ε into Equation 10.

To obtain Equation 10 a volume filled with spheres with equal diameters was considered. The number of spheres representing electrolyte decreases proportionally with the effective electrolyte void fraction. Thus s is proportional to ε.

A sphere filled with electrolyte offers no surface to its adjacent sphere, also filled with electrolyte, since for each sphere a part, ε, of its surface is occupied by spheres filled with electrolyte; the remaining part of surface area, occupied by gas or solid, will be $(1 - \varepsilon)$. Thus the total surface of gas and solid, in contact with electrolyte, is proportional to the product of first the number (proportional to ε) of electrolyte spheres and second the specific surface of gas and solid per sphere (proportional to $(1 - \varepsilon)$).

Substituting 10 into 9 gives Equation 11 whereas substitution of 11 into 4 leads to Equation 12

$$v_p = \{s_0(1 - \varepsilon)\}^{-1} \tag{11}$$

$$P = \frac{B}{\{d\eta\}} = v_p^2 \frac{R_0/R_d}{k\{d\eta\}} = \frac{R_0/R_d}{k\{d\eta\}\{s_0(1 - \varepsilon)\}^2} \tag{12}$$

Thus hydrodynamic permeability can be predicted, provided ohmic voltage drop over the diaphragm, thickness and standard specific surface of the diaphragm are known.

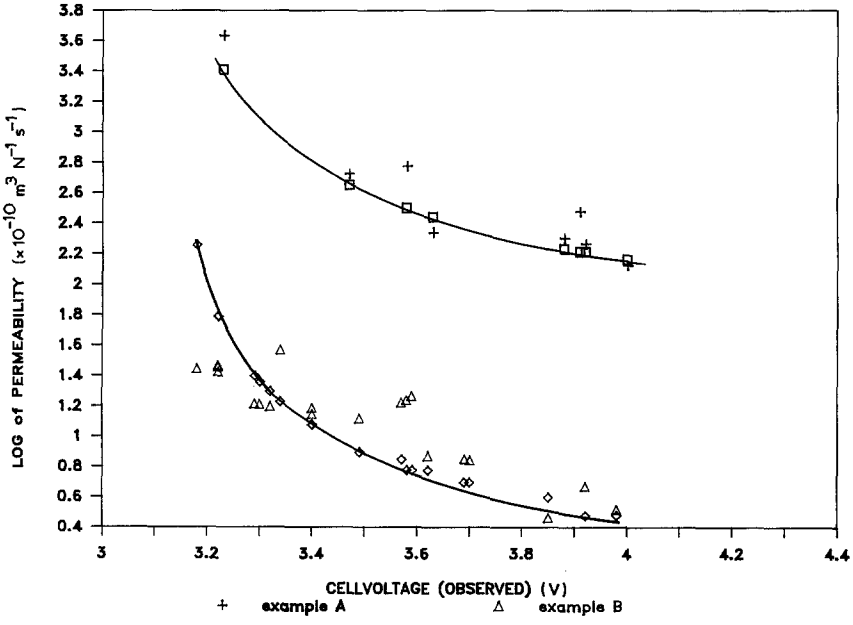

Fig. 5. Observed cell voltage versus the logarithm of observed hydrodynamic permeability.

Figure 5 presents the observed cell voltages versus the logarithm of the observed hydrodynamic permeabilities for two non-asbestos diaphragms. Both diaphragms were 1 mm in thickness and were operated at $2\,kA\,m^{-2}$. For both diaphragms time-dependent properties were observed. Figure 5 presents the predicted interrelation between observed cell voltage and hydrodynamic permeability. Typical data on the pore radius obtained by mercury porosimetry are: example A, average radius 1 μm; example B, average radius 5 μm. Observations thus show the interrelation, at a given average pore radius, of cell voltage and hydrodynamic permeability. The lines in Fig. 5 represent the calculated interrelation between cell voltage and hydrodynamic permeability (according to Equation 12 and Equations 8, 1 and 2). There is a good agreement between calculated and observed results.

This graph clearly supports Equation 4 that predicts only one parameter capable of adjusting hydrodynamic permeability to its target range of 1 to $2 \times 10^{-9}\,m^3\,N^{-1}\,s^{-1}$ (at a given diaphragm thickness and cell voltage). This unique parameter is the pore radius.

6.2. *Current efficiency and pore diameter distribution*

As discussed in previous sections, current efficiency depends, at a given current density, on: (i) brine flow rate; (ii) diaphragm thickness; (iii) pore diameter distribution. The effects of the pore diameter distribution on current efficiency are, at present, not well understood. A highly similar problem on heat and mass transfer at low Peclet numbers in porous media was treated by Schlunder [21]. As the Peclet number ($vs^{-1}\,D_3^{-1}$) of flow in diaphragms is 4×10^{-4}, which is also extremely low, his concept of porous structures, consisting of bundles of capillaries of different radii, was chosen to describe the phenomena studied.

The diaphragm (Fig. 6) is assumed to be composed of bundles of capillaries of two different diameters. In the small pores liquid velocity is low and, thus, there is an almost unhindered transport of hydroxyl ions, due to concentration gradient and electric field, from catholyte to anolyte. The large pores permit electrolyte to flow from anolyte to catholyte. Due to the electrolyte movement hydroxyl ions are flushed quantitatively backwards to the catholyte. Such a diaphragm would not be expected to have current efficiencies close to 100%. Therefore it was assumed that the diaphragm (Fig. 7) consists of a series of layers each composed of the same type of randomly mixed bundles of pores with the additional assumption of a fully established equilibration of concentrations by mixing in between each pair of layers. The effective length of pores between two points of interconnection with other pores is a new parameter which is introduced by this additional assumption.

6.2.1. Mathematics of the one-layer model. Inside the small pores liquid velocity is assumed to be zero. Inside the large pores liquid velocity is assumed to be high. Equation 6 can thus be separated into two equations.

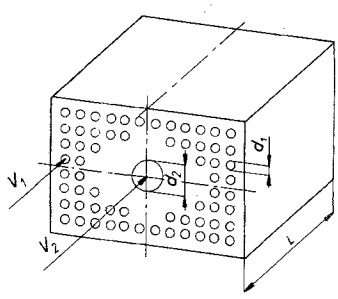

Fig. 6. The concept of a porous structure consisting of bundles of capillaries.

The diffusional and migrational flux F_3 in small pores is presented by

$$F_3 = -k_{3,1}\frac{\partial c_3}{\partial x} - k_{3,1}k_2c_3 \qquad (13)$$

The total flux N_3 is composed of this diffusional and migrational flux counteracted by the convective flow inside the large pores

$$N_3 = F_3 + uc_1 = \frac{-j(100 - CE)}{100F} \qquad (14)$$

F_3 is the flux of hydroxyl ions inside the small pores assuming liquid velocity inside these small pores to be zero. N_3 represents the total flux of hydroxyl ions inside the porous structure, neglecting migration and diffusion in the large pores. k_1 and k_2 are constants which are introduced for ease of notation. They represent, essentially, the diffusion constant and the potential gradient.

$$k_{3,1} = \frac{\varepsilon D_3}{\tau} \quad \text{and} \quad k_2 = \frac{\tau F\partial E}{RT\partial x} = \frac{FjR_0}{RT\varepsilon^2} \qquad (15)$$

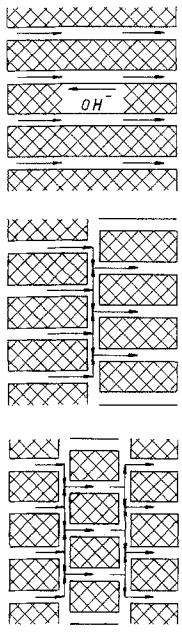

Fig. 7. The one-, two- and three-layer models.

Boundary conditions to Equation 13 are

$$x = 0; \quad c_3 = 0$$

$$x = d; \quad c_3 = c_k$$

and solving Equation 13 leads to

$$F_3 = \frac{k_{3,1}k_2\{-c_k\}}{\{1 - \exp(-k_2 d)\}} \tag{16}$$

with

$$N_3 = F_3 + uc_0 = F_3$$

Thus, according to Equation 14, when a diaphragm can be represented by the one-layer model, current efficiency is given by

$$\mathrm{CE} = 100\,\frac{\{1 - Fk_{3,1}k_2(-c_k)\}}{j\{1 - \exp(-k_2 d)\}} \tag{17}$$

6.2.2. Mathematics of the two- and multilayer models. Mass transfer in the first layer of the two-layer model is described by

$$F_{1,3} = \frac{k_{3,1}k_2\{-c_m\}}{\{1 - \exp(-k_2 d/2)\}} \tag{18}$$

$$N_{1,3} = F_{1,3} + uc_0 = F_{1,3} = \frac{-j(100 - \mathrm{CE})}{100F}$$

Solving Equation 15 over the second layer of two leads to

$$F_{2,3} = \frac{k_{3,1}k_2\{c_m \exp(-k_2\beta) - c_k\}}{\{1 - \exp(-k_2\beta)\}} \tag{19}$$

$$N_{2,3} = F_{2,3} + uc_m = \frac{-j(100 - \mathrm{CE})}{100F}$$

where c_0 = hydroxyl ion concentration in anolyte; c_m = hydroxyl ion concentration in mixing layer; c_k = concentration in catholyte. As $N_{1,3}$ has to be equal to $N_{2,3}$ these equations can be solved resulting in a calculated value of c_m and $N_{1,3}$. Similar equations describe the three-layer and the multilayer model.

In the case of the multilayer model the subscript m in Equation 19 should be replaced by j, which indicates layer j of N layers. Subscript k should be replaced by j + 1. Layer thickness β will be d/N instead of $d/2$. The calculation involves a step-by-step solving of modified Equation 19, starting from the anolyte surface in the direction of the catholyte surface of the diaphragm.

Table 2. Calculated current efficiency of a diaphragm of increasing thickness

Thickness (mm)	*One layer (%)*	*Two layers (%)*	*Three layers (%)*
1	26	47	54
2	56	75	82
3	66	84	89
4	69	90	93

Current density, 2 kA m^{-2}; effective electrolyte void fraction, 50%; c_k = 3 mol l^{-1}.

Table 3. Some results of calculated current efficiency versus effective electrolyte void fraction

Current density (A m^{-2})	2000	2000	2000	2000
Thickness (mm)	1	1.5	2	2
Caustic conc. (mol l^{-1})	2.8	3.1	3.1	3.4
Effective electrolyte void fraction (%)				
15	88	86	91	92
25	87	95	97	96
35	90	95	97	96
45	87	93	96	95
55	84	91	95	92

As can be seen from Table 2, increasing the thickness of the diaphragm and especially increasing the number of layers reduces the mass transfer of hydroxyl ions. This model thus stresses the importance of interconnections between pores in order to overcome the negative effects of liquid velocity distribution.

6.2.3. The number of layers. The multilayer model was tested against all available data obtained on asbestos diaphragms. In those diaphragms the number of layers is described by

$$N = \frac{d\varepsilon}{8u} \tag{20}$$

This equation is certainly not applicable to all non-asbestos diaphragms, because of differences in the structure of the diaphragms. Therefore, with the help of the multilayer model an estimate of the influence of the effective electrolyte void fraction on current efficiency was made. Results are shown in Table 3. It was found that: (i) increasing the effective electrolyte void fraction favours diffusion of hydroxyl ions and thus decreases current efficiency; (ii) decreasing the effective electrolyte void fraction increases the potential gradient inside the diaphragm; however, total current remains constant and, if the part of current which is transported by hydroxyl ions is constant, then the mass transfer by migration will be independent of the effective electrolyte void fraction; (iii) increasing the effective electrolyte void fraction will increase, according to Equation 20, the number of layers; this effect favours current efficiency.

All calculations were based on diffusion coefficients by Caldwell *et al.* [22].

Figure 8 presents a comparison of calculated results with observed current efficiencies of examples A and B of Figs 4 and 5. All data refer to 1-mm diaphragms at 2 kA m^{-2} and 120–124 g l^{-1} caustic. The effective electrolyte void fraction of the experimental values was obtained from observed hydrodynamic permeability and the known standard specific surface according to Equation 12. The shape of the observed and calculated curves is very similar.

The observed and calculated curves share in common: a maximum in current efficiency in the range from 20 to 40% effective electrolyte void fraction; a sharp decline in current efficiency below 20%; a slight decline above 40%.

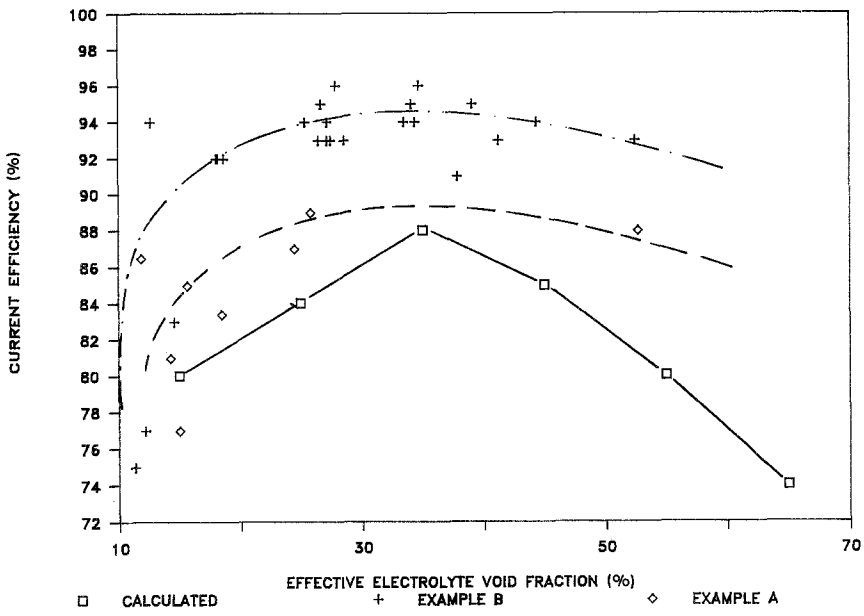

Fig. 8. Calculated current efficiency versus effective electrolyte void fraction at $2\,kA\,m^{-2}$ and $124\,g\,l^{-1}$ caustic. A comparison of calculations and experiment.

There are two sets of experimental data showing the highest current efficiencies on the diaphragm with 1-μm pores. The two experimental curves show, at the same effective electrolyte void fraction, differences of 10% in current efficiency. These differences, and the difference towards the calculated curve, are explicable in terms of differences in number of layers between the two diaphragms and the usage (in the calculations) of the erroneous Equation 20.

7. Conclusion

From zirconia and PTFE, mixed and treated in the appropriate manner, chemically and mechanically stable non-asbestos diaphragms for service in chlor-alkali cells can be produced.

In this paper it is shown that such diaphragms should:

- show, in order to obtain as many layers as possible, a porous structure with as many interconnections between pores as possible; a structure with an effective length between two interconnections of 1–5 μm (asbestos fibre thickness) is preferred
- have a thickness of 2–3 mm
- show good and stable wetting by the electrolyte
- have an effective electrolyte void fraction of 40% or even slightly more; as current efficiency is shown (by experiment) to be, to some extent, uninfluenced by the effective electrolyte void fraction whereas cell voltage strongly decreases with increasing effective electrolyte void fraction, a decrease of power consumption with increasing effective electrolyte void fraction is predicted

As asbestos diaphragms show a hydrodynamic permeability of 1 to $2 \times 10^{-9}\,m^3\,N^{-1}\,s^{-1}$ and in order to obtain the desired similar or even better performance on hydrodynamic permeability and cell voltage compared to asbestos diaphragms, the hydraulic radius should be 0.1–0.5 μm. Thus the standard specific surface of the solids in the structure should be $10^7\,m^{-1}$.

References

[1] P. Vermeiren and R. Leysen, Poster presented at 38th ISE Meeting, Maastricht (1987).
[2] L. C. Curlin, T. F. Florkiewicz and R. Matousek, Paper presented at Chlorine Symposium, London, June (1988) (to be published) Ellis Horwood, London.
[3] S. F. Kelham, *I. Chem. E. Symp. Ser.* **89** (1986) 235.
[4] W. Kramer, Brochure Uhde MembranZellen.
[5] F. Hine, *Electrochim. Acta* **22** (1977) 429.
[6] D. L. Caldwell, 'Comprehensive Treatise on Electrochemistry', Plenum Press, New York (1981) Vol. 2, pp. 105–161.
[7] M. S. Kirchner, 'Chlorine ACS Monograph 154' (edited by J. C. Sconce), Reinhold, (1955) pp. 105–125.
[8] I. V. Kadija, EPA 0.048.775.
[9] G. C. Byrd, EPA 0.008.165.
[10] J. J. H. Krause, EPA 0.002.894.
[11] J. Bachot, EPA 0.033.262.
[12] T. Mukaibo, *J. Electrochem. Soc. Japan* **20** (1952) 482.
[13] D. A. Bruggeman, *Ann. Physik* **24** (1935) 636.
[14] R. E. Meredith and C. W. Tobias, 'Advances in Electrochemical Engineering and Electrochemistry', (edited by C. W. Tobias), Interscience Publishers, Vol. 2, pp. 15–47.
[15] R. B. MacMullin and G. A. Muccini, *AIChE J.* **2** (1956) 393.
[16] R. E. White and J. van Zee, *J. Electrochem. Soc.* **132** (1985) 818.
[17] R. E. White, J. S. Beckerdite and J. van Zee, 'Electrochemical Cell Design', (edited by R. E. White), Plenum Press, New York (1983) pp. 25–60.
[18] C. A. Lazarz, DP 29.44.251.
[19] C. A. Lazarz, DP 3.110.322.
[20] E. H. Cook and C. A. Lazarz, Paper presented to the 26th Chlorine Plant Managers Seminar, New Orleans, Feb. 2 (1983).
[21] E. U. Schlunder, *Chem. Eng. Sci.* (1977) 845.
[22] D. L. Caldwell, K. A. Poush, J. W. van Zee and R. White, Proceedings of the Symposium on Electrochemical Processes, The Electrochemical Society Inc., Pennington, NJ (1983).